Precambrian Research 313 (2018) 68–77

Contents lists available at ScienceDirect

Precambrian Research

journal homepage: www.elsevier.com/locate/precamres

Evolution of primary producers and productivity across the Ediacaran-Cambrian transition

Lei Xiang[a,b,*], Shane D. Schoepfer[c], Hua Zhang[a,b,*], Chang-qun Cao[a,b], Shu-zhong Shen[a,b]

[a] State Key Laboratory of Palaeobiology and Stratigraphy, Nanjing Institute of Geology and Palaeontology and Center for Excellence in Life and Paleoenvironment, Chinese Academy of Sciences, 39 East Beijing Road, Nanjing 210008, China
[b] Center for Research and Education on Biological Evolution and Environment, Nanjing University, 163 Xianlin Avenue, Nanjing 210023, China
[c] Department of Geosciences and Natural Resources, Western Carolina University, 1 University Way, Cullowhee, NC 28779, USA

ARTICLE INFO

Keywords:
Kerogen
Nitrogen isotopes
Nutrient limitation
Eukaryote
Cambrian Explosion

ABSTRACT

Nearly all extant animal phyla first appeared during the Ediacaran-Cambrian transition. A revolution in primary producer ecology and marine productivity has been proposed as a bottom-up ecological driver for this rapid diversification of metazoans. However, the control(s) driving the evolution of primary producers and primary productivity around the Ediacaran-Cambrian transition, and their potential relationship to the Cambrian Explosion, are not fully understood. In this study, we measured the nitrogen content and the nitrogen isotopic composition of kerogen in the Piyuancun and Hetang Formations, using samples collected from the Chunye-1 well, on the Lower Yangtze Block in western Zhejiang. Our isotope results suggest that nitrate was the dominant N source fueling primary productivity during deposition of the entire Piyuancun Formation and lower Hetang Formation, with only a minor contribution from N_2 fixation. Quantitative reconstructions of paleoproductivity based on organic carbon and pyrite content and sedimentation rate indicate that productivity either stayed the same or increased during the transition from the Piyuancun Formation to the overlying Hetang Formation. Thus, fixed N availability was not the ultimate factor limiting primary productivity during the Ediacaran-Cambrian transition. Combining our data with published nitrogen isotope records from the Early-Middle Ediacaran to Cambrian Stage 4 suggests that NO_3^- was the dominant N species fueling phytoplanktonic productivity during the broad Cambrian Explosion interval, from its earliest roots in the Ediacaran through the main episode in Cambrian Stage 3. Eukaryotes lack the ability to fix nitrogen, and preferentially assimilate nitrate. The NO_3^--dominated euphotic zone from the Early-Middle Ediacaran to Cambrian Stage 3 may have promoted the radiation of relatively large eukaryote phytoplankton, which may have been an important driver of early animal diversification.

1. Introduction

The astonishing evolutionary burst in animal diversity known as the Cambrian Explosion was rooted in the Ediacaran, but did not reach its peak until Stage 3 of Cambrian Series 2 (Erwin et al., 2011; Na and Kiessling, 2015; Zhu et al., 2017). By that time, a complex ecological structure, with food webs resembling those of the later Phanerozoic, had been established (Mángano and Buatois, 2014). Photosynthesis by phytoplankton would be the ultimate source of the food and oxygen fueling this rise in animal diversity (Knoll and Nowak, 2017). The evolution of primary producers, and changes in the rate of primary productivity around the Ediacaran-Cambrian transition, may have played an important role in the explosive diversification of animals (Knoll, 2017).

The rate of photosynthesis is governed by the availability and stoichiometry of nutrient elements, such as nitrogen and phosphorus (Moore et al., 2013). There is persistent controversy over whether nitrogen can act as the ultimate limiting nutrient over geologic timescales, particularly during intervals of widespread marine anoxia (Falkowski, 1997; Tyrrell, 1999; Saltzman, 2005); the behavior of marine nitrogen may have been a key element in the expansion of animal diversity. Sedimentary organic N isotopes typically reflect the availability, type, and isotopic composition of fixed N in the euphotic zone, and the $\delta^{15}N$ of sedimentary kerogen may be a reliable proxy for the $\delta^{15}N$ of primary-producer biomass (Beaumont and Robert, 1999; Godfrey and Falkowski, 2009). Previous nitrogen isotope studies of the

* Corresponding authors at: State Key Laboratory of Palaeobiology and Stratigraphy, Nanjing Institute of Geology and Palaeontology and Center for Excellence in Life and Paleoenvironment, Chinese Academy of Sciences, 39 East Beijing Road, Nanjing 210008, China.
E-mail addresses: leixiang@nigpas.ac.cn (L. Xiang), hzhang@nigpas.ac.cn (H. Zhang).

https://doi.org/10.1016/j.precamres.2018.05.023
Received 4 January 2018; Received in revised form 12 May 2018; Accepted 16 May 2018
Available online 17 May 2018
0301-9268/

Ediacaran-Cambrian interval in South China have focused mainly on the relatively shallow-water sediments of the upper and middle Yangtze Block (Cremonese et al., 2013, 2014; Ader et al., 2014; Kikumoto et al., 2014; Wang et al., 2013, 2015, 2017; Hammarlund et al., 2017; Zhang et al., 2017).

In order to understand the environmental controls on the evolution of primary productivity and primary producer diversity during the Ediacaran-Cambrian transition, we studied nitrogen isotopes in the basinal sediments of the lower Yangtze Block, by examining a core from the Chunye-1 well. This core represents a continuous sedimentary succession spanning from the Late Ediacaran through Cambrian Stage 4, and we were able to sample the entirety of the Piyuancun and Hetang Formations. Measurements of total nitrogen content (TN) and the nitrogen isotope composition of kerogen ($\delta^{15}N_{kero}$) were used to explore the temporal evolution and controls on primary productivity, with the aim of better understanding the relationship between bottom-up ecological drivers of eukaryote evolution and the Cambrian Explosion.

2. Geologic setting

The Chunye-1 well is located near the village of Hengyan, in Chun'an County, Zhejiang Province, China (118°35′29.72″E, 29°25′19.44″N, Fig. 1a–c). The well was originally drilled for shale gas exploration, to a total depth of 804.81 m. The recovered core consists of the Lantian, Piyuancun, Hetang, Dachenling and Yangliugang formations, in ascending order (GBA, 1971). With the exception of an anthracite layer in the Hetang Formation, core recovery was greater than 95%. No erosional unconformities are apparent between the lowermost horizons recovered from the Lantian Formation and the top of the Hetang Formation, suggesting continuous deposition over the interval considered in this study.

The Lantian Formation consists mainly of white to light-grey, medium- to thick-bedded sandy dolostone. The lower and middle Piyuancun Formation are composed of grey to black, medium- to thick-bedded cherts, interbedded with sandy dolostone and sandstone, while the upper part of the Piyuancun Formation is composed of grey to black, medium-bedded limestone. The Hetang Formation consists primarily of black, thin-bedded carbonaceous mudstones, shales, and anthracite, interbedded with lenticular limestones and phosphorites. The Hetang Formation is conformable with the overlying Dachenling Formation, which consists mainly of limestone.

During the Ediacaran-Cambrian transition, depositional environments on the Yangtze Block ranged from shallow-water platform carbonates and phosphorites to deep slope and basin environments (Jiang et al., 2012, Fig. 1a). Previous studies have suggested that the western Zhejiang area was a gulf (termed the Qiantang Gulf, Fig. 1b), which was bounded by the Jiangnan Oldland along its western margin and the Cathaysian Oldland along its southeastern margin (Xue and Yu, 1979; Huang and Zhang, 1988). The basement underlying the Qiantang Gulf was cut by a set of northeast-southwest striking faults, dividing it into four fault blocks, referred to (from NW to SE) as the Changxing-Hangzhou, Anji-Kaihua, Tonglu-Jiande, and Zhuji-Quxian blocks (Huang and Zhang, 1988). Of these, the Anji-Kaihua Block has the thickest sedimentary cover, and preserves the most complete sedimentary succession (Xue and Yu, 1979; Huang and Zhang, 1988). These sediments were primarily derived from the Jiangnan Oldland, which was subaerially exposed to the west (Fig. 1b). The Chunye-1 well is located in the southwestern part of the Anji-Kaihua fault block (Fig. 1b).

Lithostratigraphic and chemostratigraphic correlation suggests that the Piyuancun Fm. in the Chunye-1 well represents a relatively long interval of time, ranging from the Late Ediacaran through Cambrian Stages 1–3. The basal Hetang Fm. in the Chunye-1 well dates to the late Qiongzhusian (late Cambrian Stage 3) at the earliest, and the upper Hetang Fm. very likely represents the Canglangpuian stage (Cambrian Stage 4, Xiang et al., 2017).

3. Sampling and methods

A total of 132 samples were collected from a 300 m interval of the Chunye-1 well, spanning from the basal Piyuancun Formation to the uppermost Hetang Formation. These samples were broken into small pieces (diameter ~2 mm) by hammer. Individual pieces were then selected for pulverization, avoiding carbonate and pyrite fracture fills, veins, and nodules. The pieces (> 50 g) were powdered using a SPEX 8515 Shatterbox with a ceramic insert.

Total nitrogen content and the nitrogen isotope composition of organic residues were both measured using a modified elemental analysis-isotope ratio mass spectrometry (EA-IRMS) procedure (CEEA1112 CNS Analyzer, interfaced with a DELTA plus XL mass spectrometer), at the Guangzhou Institute of Geochemistry, Chinese Academy of Sciences. The details of this method and the analytical system, are described in Li and Jia (2011).

Powdered samples were digested with heated 6 N HCl, then a mixture of 6 N HCl and 40% HF, followed by a final treatment with 6 N HCl, to remove carbonate and silicates. After the residue was rinsed in distilled water and concentrated by centrifugation, kerogen was separated from secondary fluoride precipitates by heavy liquid separation, using ZnBr with a density of 2.0 g/cm^3 (Cai et al., 2009; Kump et al., 2011). The measured C/N ratios of kerogen samples were scaled to the TOC content of the bulk sample, to calculate the abundance of kerogen-bound nitrogen. Nitrogen isotope measurements were corrected for a procedural N_2 blank, and reference gases were calibrated with the 3-point method, relative to IAEA standards Urea 1 ($\delta^{15}N$ = 0.4‰), Urea 2 ($\delta^{15}N$ = 20.1‰), and N3 ($\delta^{15}N$ = 5.0‰). Results are reported in standard delta notation, relative to atmospheric air. Reproducibility was ± 0.5‰ for $\delta^{15}N$.

4. Results and discussion

4.1. Carbon and nitrogen measurements

Kerogen $\delta^{15}N$ values are generally > 1‰ throughout the entirety of the Piyuancun Formation, with sporadic samples yielding values of < 1‰. The Hetang Formation can be divided into two intervals (the lower Hetang Formation and middle-upper Hetang Formation) based on $\delta^{15}N_{kero}$ values. In the lower Hetang Formation (594.46 m–563.29 m), $\delta^{15}N_{kero}$ values are mainly > 1‰, while those in the middle-upper Hetang Formation (559.44 m–407.76 m) are typically < 1‰. (Table S1, Fig. 2). The C/N ratios of kerogen $(C/N)_{kero}$ in the Chunye-1 well were generally high, fluctuating between 33 and 630. Like $\delta^{15}N_{kero}$ values, average $(C/N)_{kero}$ ratios were higher in the Piyuancun Formation and lower Hetang Formation (305) than in the middle-upper Hetang Formation (213, Fig. 2, Table S1).

The majority of variability in $\delta^{15}N_{kero}$ is seen in samples with low organic carbon (Fig. 3a) and nitrogen (Fig. 3b) content, with $\delta^{15}N_{kero}$ values converging in the −2 to +1‰ range in more organic rich samples. The average molar H/C ratios of kerogen from the Piyuancun and Hetang Formations in the neighboring Diben section (~25 km southwest; Fig. 1b), were 0.33 and 0.30 respectively (Yuan et al., 2014). Thus, our studied interval may also be at prehnite-pumpellyite facies, where partitioning of nitrogen between organic and mineral phases typically results in < 2‰ of fractionation (Stüeken et al., 2017). Although the C/N ratios of kerogen in Chunye-1 well were generally higher than 100, they show little correlation with $\delta^{15}N_{kero}$ (Fig. 3c, R2 = 0.15), suggesting that $\delta^{15}N_{kero}$ has not been strongly influenced by thermal maturation processes or the addition of ^{15}N-enriched fluids during metasomatism (Kump et al., 2011).

In modern low-oxygen, organic-rich oceanic water masses, little difference in $\delta^{15}N$ composition is observed between sinking particles and surface sediments, allowing the effect of biodegradation on the $\delta^{15}N$ of organic matter to be ignored when interpreting $\delta^{15}N$ data (Robinson et al., 2012). Iron speciation and redox sensitive trace metal

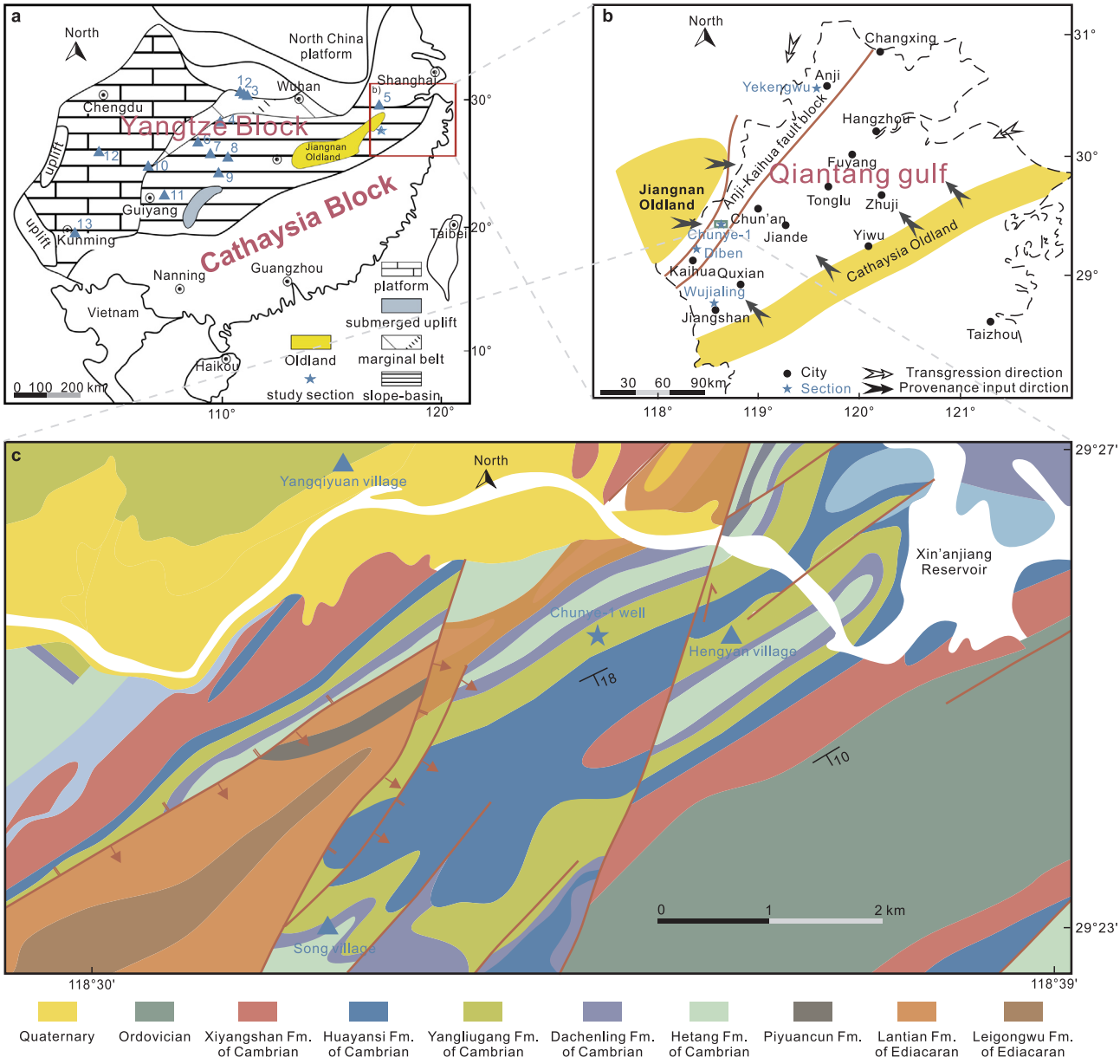

Fig. 1. a) Reconstructed paleogeography of the Yangtze Block during the Late Ediacaran and Cambrian Stage 1 (Modified from Jiang et al., 2012); published stratigraphic sections include: 1–Jijiawan-Wuhe, 2–Three Gorges drill core, 3–Yangjiaping, 4–Sancha, 5–Lantian drill core, 6–Huanglian, 7–Longbizui, 8–Yanwutan-Lijiatuo, 9–Yuanjia, 10–Maoshi-Zhongnan, 11-Nangao, 12–Xiaotan, and 13–Chengjiang; b) detailed paleogeographic map of the Qiantang Gulf during the Late Ediacaran to Cambrian Stage 4 (Modified from Xue and Yu, 1979; Huang and Zhang, 1988); c) geologic map of the area surrounding the Chunye-1 well (Modified from GBA, 1971).

proxies indicate that conditions were consistently anoxic during deposition of the Piyuancun and Hetang Formations in the Chunye-1 well (Fig. 2, Xiang et al., 2017), and thus the effects of biodegradation on our measured $\delta^{15}N$ are likely to be very small.

4.2. Evolution of N sources fueling primary productivity

An aerobic nitrogen cycle, involving nitrification, denitrification, and microbial N fixation was already in place prior to the Neoproterozoic (Stüeken et al., 2015; Zerkle et al., 2017). Measured $\delta^{15}N_{kero}$ values in the Piyuancun Formation and lower Hetang Formation (707.21 m–563.29 m) ranged from −2.6‰ to 4.8‰, with an average value of 2.2 ± 1.3‰. With the exception of a few outliers, $\delta^{15}N_{kero}$ values were generally > 1‰, though lower than the mean value of modern oceanic $\delta^{15}NNO_3^-$ (~5‰, Sigman and Casciotti, 2001), which reflects the isotopic fractionation associated with water column denitrification. The $\delta^{15}N$ of nitrogen fixed by marine diazotrophs using Mo-based nitrogenases usually falls between −2‰ and +1‰ (Zhang et al., 2014; Stüeken et al., 2015), reflecting the isotopic composition of atmospheric nitrogen (0‰). Diazotrophs using alternative, V- and Fe-based nitrogenases can fractionate nitrogen by −6‰ to −8‰ relative to the atmosphere, with a wide range of isotopic variability (Zhang et al., 2014; Stüeken et al., 2015). Thus, we interpret the nitrogen isotope values seen in the Piyuancun Formation and lower Hetang Formation to reflect a photic-zone nitrogen cycle dominated by dissolved NO_3^-, but also including a minor component of N fixed directly from the atmosphere (Junium and Arthur, 2007; Koehler et al., 2017). Similar, slightly positive $\delta^{15}N$ values (with an average value of 1.3‰) have been reported from the Late Ediacaran-through Cambrian Stages 1–3 across South China (Cremonese et al., 2013, 2014; Kikumoto

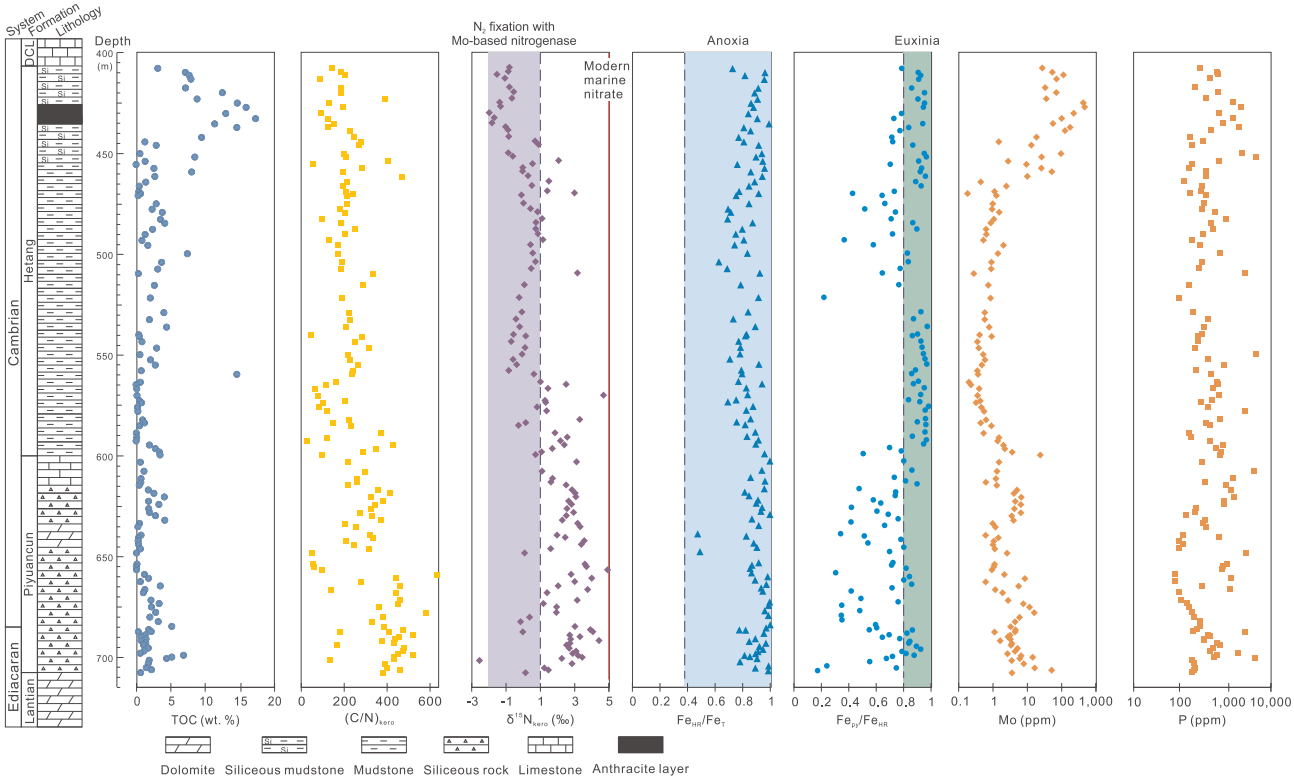

Fig. 2. Stratigraphic distribution of TOC content, the $(C/N)_{kero}$ ratio, $\delta^{15}N_{kero}$, the Fe_{HR}/Fe_T ratio, the Fe_{py}/Fe_{HR} ratio, Mo content, and P content in the Chunye-1 well. Note that Mo and P content are presented on a logarithmic scale.

et al., 2014; Hammarlund et al., 2017), indicating a similar mix of nitrogen sources to the euphotic zone.

Measured $\delta^{15}N_{kero}$ values in the middle and upper Hetang Formation (559.44 m–407.76 m) range from −2.0‰ to 3.1‰, with an average value of 0 ± 1.0‰. This small range of variability in $\delta^{15}N_{kero}$, centered around 0‰, suggests that the N fueling primary producers was sourced mainly from microbial N_2 fixation, using Mo-based nitrogenase enzymes. The marked decrease in average $(C/N)_{kero}$ ratios, from 305 in the Piyuancun Formation and lower Hetang Formation, to 213 in the middle-upper Hetang Formation, is consistent with the ecological replacement of nitrate-assimilating phytoplankton by diazotrophs with lower C/N ratios (Kunimitsu et al., 2009).

Alternative V- and Fe-based nitrogenases are predicted to become active when the concentration of dissolved Mo drops to below 1 nM (Glass et al., 2010; Stüeken et al., 2015). The oceanic Mo reservoir appears to have been low during deposition of the middle Hetang Formation (559.44 m and 528.81 m), with little to no trace element enrichment in sediments despite the expansion of sulfidic water masses (Xiang et al., 2017). Nevertheless, Mo fluxes remained high enough for Mo-based nitrogenases to operate in the surface mixed layer (Anbar and Knoll, 2002). This may be due to redox stratification, maintained by high organic export (Ader et al., 2016), and enhanced riverine Mo input as continental oxidative weathering after the Neoproterozoic Oxygenation Event (NOE, Knoll and Nowak, 2017; Scott et al., 2008).

Iron speciation and trace element proxies suggest that the Hetang Formation was deposited under alternatively ferruginous and euxinic conditions, and that anoxic water masses expanded during deposition of the lower and middle Hetang Formation (594.46 m–468.91 m, Xiang et al., 2017), possibly due to enhanced export production. The acceleration of N_2 fixation in the euphotic zone thus occurred slightly later than this expansion of anoxic deepwater. Both processes may be rooted in the gradual increase in global tectonic activity and weathering of the continental crust from 525 Ma (Squire et al., 2006), and consequent increase in the riverine flux of P and other nutrients. This could have driven the observed increase in nitrogen fixation by lowering oceanic N:P ratios below the Redfieldian 16:1, and requiring N_2 fixation to restore the balance (Tyrrell, 1999), while promoting deepwater anoxia through the export of organic carbon. Trace element data indicate the regional or global expansion of oxic waters during deposition of the upper Hetang Formation (466.21 m–407.76 m, Xiang et al., 2017). As more of the ocean became oxic, it may have accumulated a larger standing reservoir of dissolved trace metals, including cofactors such as Mo necessary for N fixation (Xiang et al., 2017), and further promoting diazotrophy.

4.3. Quantitative reconstruction of primary productivity

While primary productivity in the photic zone is the ultimate source of organic carbon in marine sediments, the proportion of primary productivity that is ultimately preserved is a function of several variables. Both sinking organic matter in the water column and organic carbon buried in sediments are subject to multiple preservation effects, governed by heterotrophic respiration, sedimentation rate, and thermal maturation (Algeo et al., 2013). Average TOC values in the Piyuancun and Hetang Formations are 1.77% and 4.14%, respectively, while average S_{py} values are 0.88% and 2.71%, respectively. Raiswell and Canfield (2012) determined that the precipitation of 1 mol of pyrite consumes ~4 mol of organic matter; assuming some loss of dissolved H_2S under euxinic conditions, and the sequestration of sulfide by other metal cations, we calculate that the precipitation of 1 g of S_{py} represents the decomposition of at least 0.75 g of organic carbon. This relationship can be used to calculate an 'original' TOC value for use in paleoproductivity equations (Table S2).

The sedimentation rate, which affects the amount of time in which deposited organic carbon is exposed to heterotrophic respiration, is another key control on carbon preservation, even in anoxic environments where the majority of respiration is likely to be anaerobic (Schoepfer et al., 2015); at high sedimentation rates, a greater

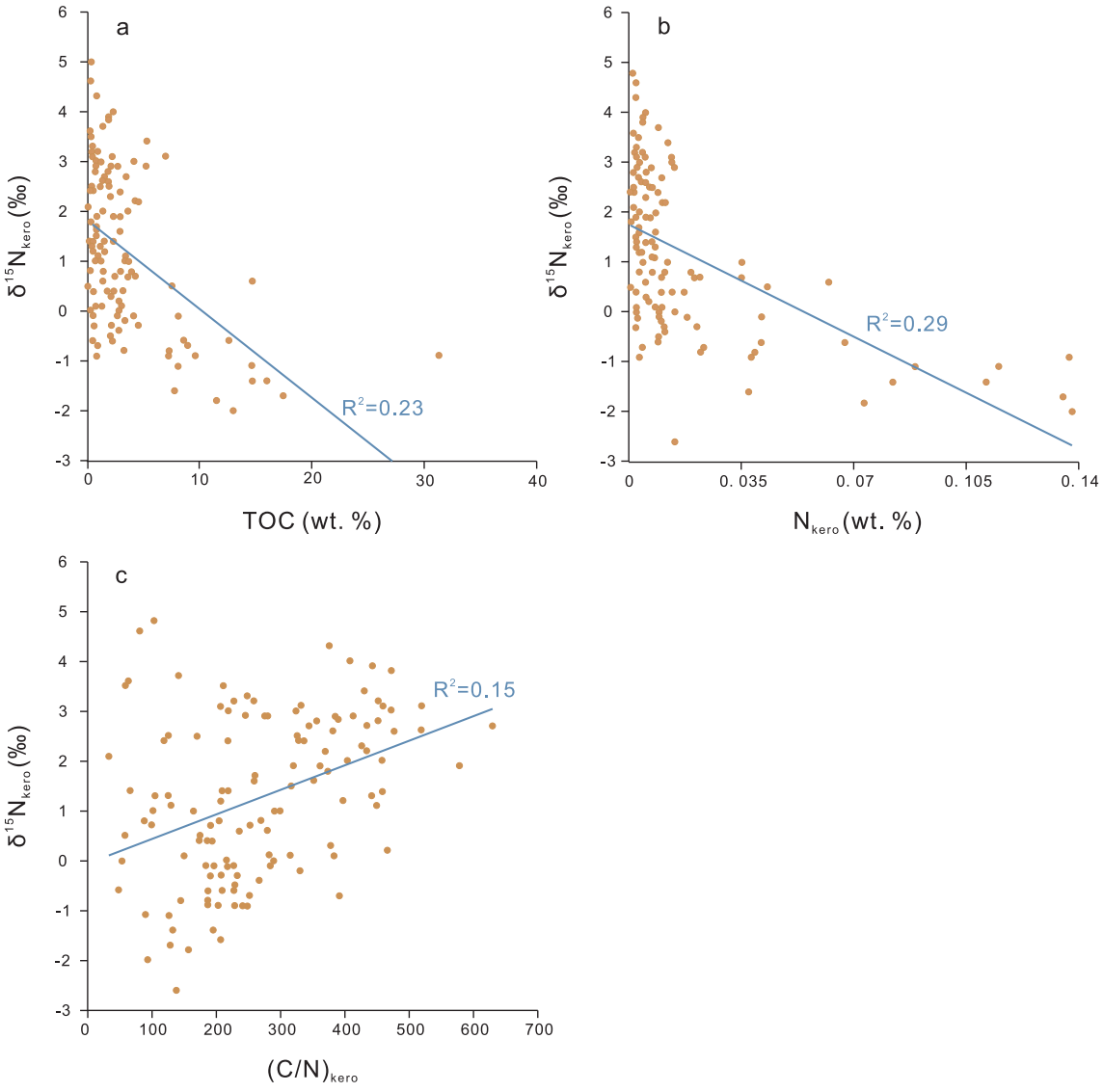

Fig. 3. Cross plots of organic geochemical measurements in the Chunye-1 well: a) TOC versus $\delta^{15}N_{kero}$; b) N content versus $\delta^{15}N_{kero}$; c) $(C/N)_{kero}$ ratio versus $\delta^{15}N_{kero}$.

proportion of produced carbon is likely to be preserved. Regional stratigraphic constraints (Xiang et al., 2017) imply that the 110.95 m-thick Piyuancun Formation spans from the Late Ediacaran (~551 Ma) to the end of Cambrian Stage 3 (~514 Ma), thus representing at least 37 Myr. In contrast, the entire 186.7 m-thick Hetang Formation was likely deposited during Cambrian Stage 4, in less than 5 Myr. Thus, applying a typical density for sedimentary rocks (2.5 g cm^{-3}), the mass accumulation rate (MAR) of the Piyuancun Formation (~0.75 g cm^{-2} kyr^{-1}, Table S2) may have been an order of magnitude lower than that of the overlying Hetang Formation (~9.34 g cm^{-2} kyr^{-1}, Table S2).

While this major increase in sedimentation rate may appear surprising, similar changes are observed across the Yangtze Block during the Ediacaran-Cambrian transition, coinciding with the transition from carbonate/phosphorite or chert units to mudstone/shale units. This is seen in the Xiaotan section on the shallow-water platform (Cremonese et al., 2013), in the Three Gorges transitional zone (Kikumoto et al., 2014), and in the Longbizui slope-basin section (Wang et al., 2012). A consistent decrease in the seawater $^{87}Sr/^{86}Sr$ ratio from 543 and 521 Ma (Maloof et al., 2010) may suggest weakened continental weathering (Peters and Gaines, 2012). At the same time, sea level was rising globally from the base of Cambrian (Haq and Schutter, 2008), resulting in highly-condensed sedimentary successions across South China during Cambrian Series 1 (Jiang et al., 2012). An increase in sedimentation rate occurs concurrently with the near-total disappearance of marine chemical sediments after Cambrian Stage 2 (Zhu et al., 2003), with sedimentation increasingly dominated by terrigenous components. Seawater $^{87}Sr/^{86}Sr$ ratios increased rapidly, to reach their maximum value over the past 900 Ma, since Cambrian Stage 3 (Maloof et al., 2010), which may reflect a globally-significant interval of enhanced continental denudation (Peters and Gaines, 2012; Squire et al., 2006).

With TOC and sedimentation rate values, we can begin to estimate paleoproductivity – due to the inherent uncertainties in these estimates (as high as 100%, Schoepfer et al. 2015), we will apply a variety of equations, and look for common trends and patterns. The equations used for calculating paleoproductivity and their derivation are described in detail in Schoepfer et al. (2015), as well as Felix (2014) and references therein; specifically, we will applying the equations of Müller and Suess (1979) and Stein (1986), which Felix (2014) found to be among the most reliable for reconstructing primary productivity. Some of these approaches attempt to subsume the various preservational effects within large datasets from a broad range of environments, establishing empirical relationships between primary productivity in the upper water column and the organic carbon accumulation rate (OCAR). Other approaches attempt to explicitly model the effects of

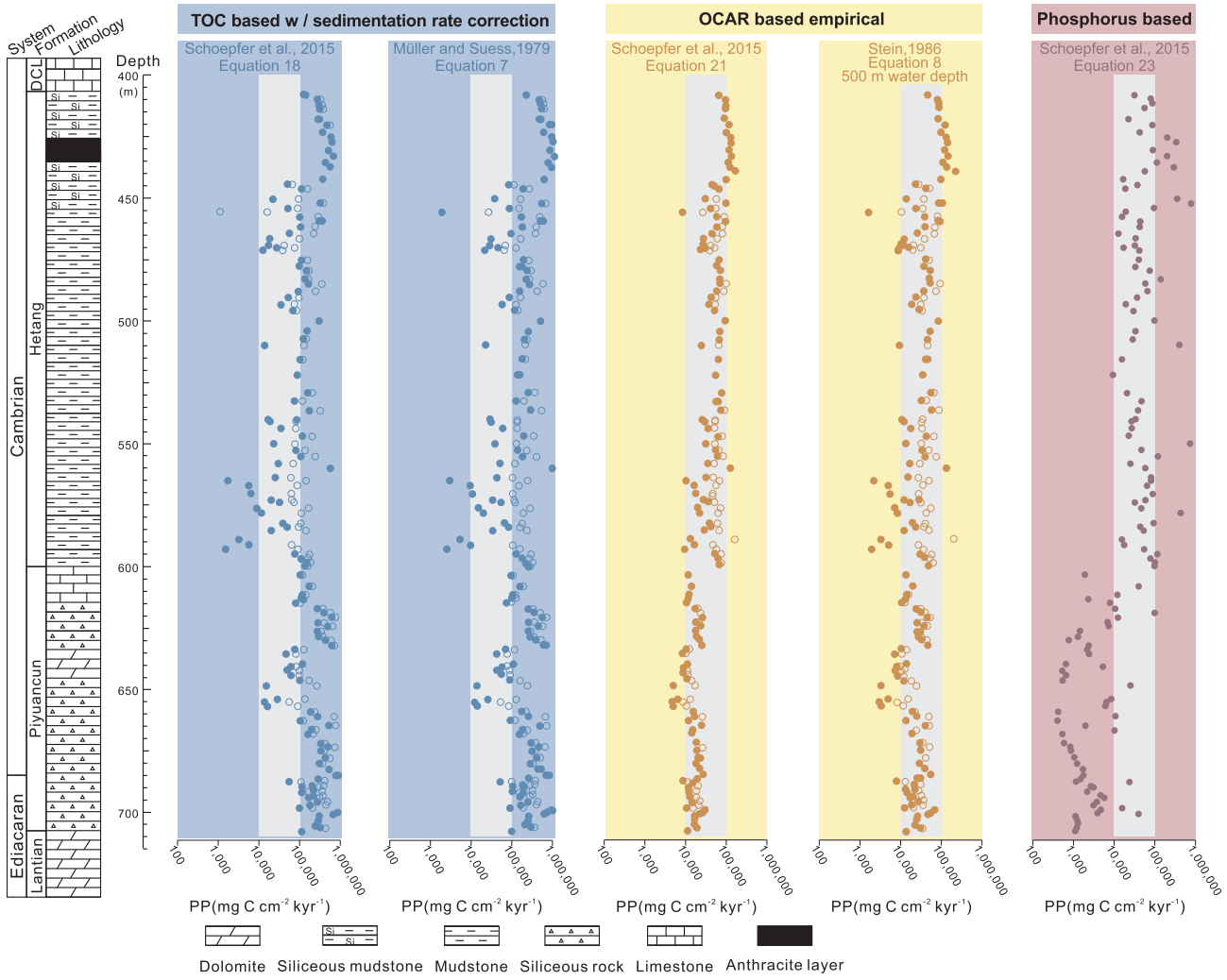

Fig. 4. Stratigraphic distribution of reconstructed paleoproductivity, using Eqs. (18), (21) and (23) from Schoepfer et al. (2015), as well as the equations of Müller and Suess (1979) and Stein (1986), in the forms presented by Felix (2014). A water depth of 500 m. was assumed for the Stein (1986) technique. Solid symbols represent primary productivity as calculated from measured TOC; hollow circles show the results of the same equations using a reconstructed original TOC value calculated as (TOC + $0.75S_{py}$). Highlighted area show the range of long-term regionally averaged productivity rates seen in the modern ocean (Longhurst et al., 1995).

carbon degradation in the water column and at the sediment water interface, and thus yield higher initial productivity values for the same TOC content at lower sedimentation rates (Felix, 2014 and references therein; Schoepfer et al. 2015).

Reconstructions using the latter approach (i.e., specifically accounting for sedimentation rate) yield quite high values for productivity in the Piyuancun Formation ($> 10^5$ mg C cm^{-2} kyr^{-1}; Fig. 4); due to the low sedimentation rate, it is assumed that the preserved TOC represents only a minute fraction of original primary productivity. Calculated productivity dips slightly in the lower and middle Hetang Formation, to values of $\sim 10^5$ mg C cm^{-2} kyr^{-1}, before returning to higher values in the organic-rich upper Hetang Formation. In general, these calculated values are quite high, with only the lower and middle Hetang Formation yielding values that overlap with long-term regional productivity averages from the modern world (Longhurst et al., 1995). While the highest values are not inherently unrealistic (similar productivity values have been observed in upwelling zones such as the California Current, see www.science.oregonstate.edu/ocean.productivity/), they likely represent an overcorrection for the low sedimentation rates seen in this system, especially in the Piyuancun Formation. Nevertheless, it is notable that even with this correction, we observe no decrease in productivity corresponding with the decline in nitrogen isotope values in the lower to middle Hetang Formation, suggesting that this does not represent a period in which nitrogen availability limited productivity to low values.

The range of paleoproductivity values calculated from the OCAR overlaps considerably with the range of values seen in the modern ocean. The Piyuancun Formation shows values of $\sim 10^4$ mg C cm^{-2} kyr^{-1}, increasing by approximately an order of magnitude to reach values of around 10^5 mg C cm^{-2} kyr^{-1} in the upper Hetang Formation (Fig. 4). Some of this increase is likely attributable to enhanced carbon preservation at high sedimentation rates, which these equations do not explicitly correct for. However, in combination with the TOC and sedimentation rate-based equations discussed above, it seems apparent that, at a minimum, primary productivity remained relatively constant over the studied interval, and may have increased considerably, especially in the upper Hetang Formation. As discussed above, this trend does not appear to be tied to changes in the nitrogen cycle.

In addition to organic carbon, phosphorus is a major component of organic matter that can be used to reconstruct paleoproductivity (Schoepfer et al., 2015), though uncertainty surrounding the controls on P preservation means that this relationship can only be empirical. Paleoproductivity values calculated from the phosphorus accumulation

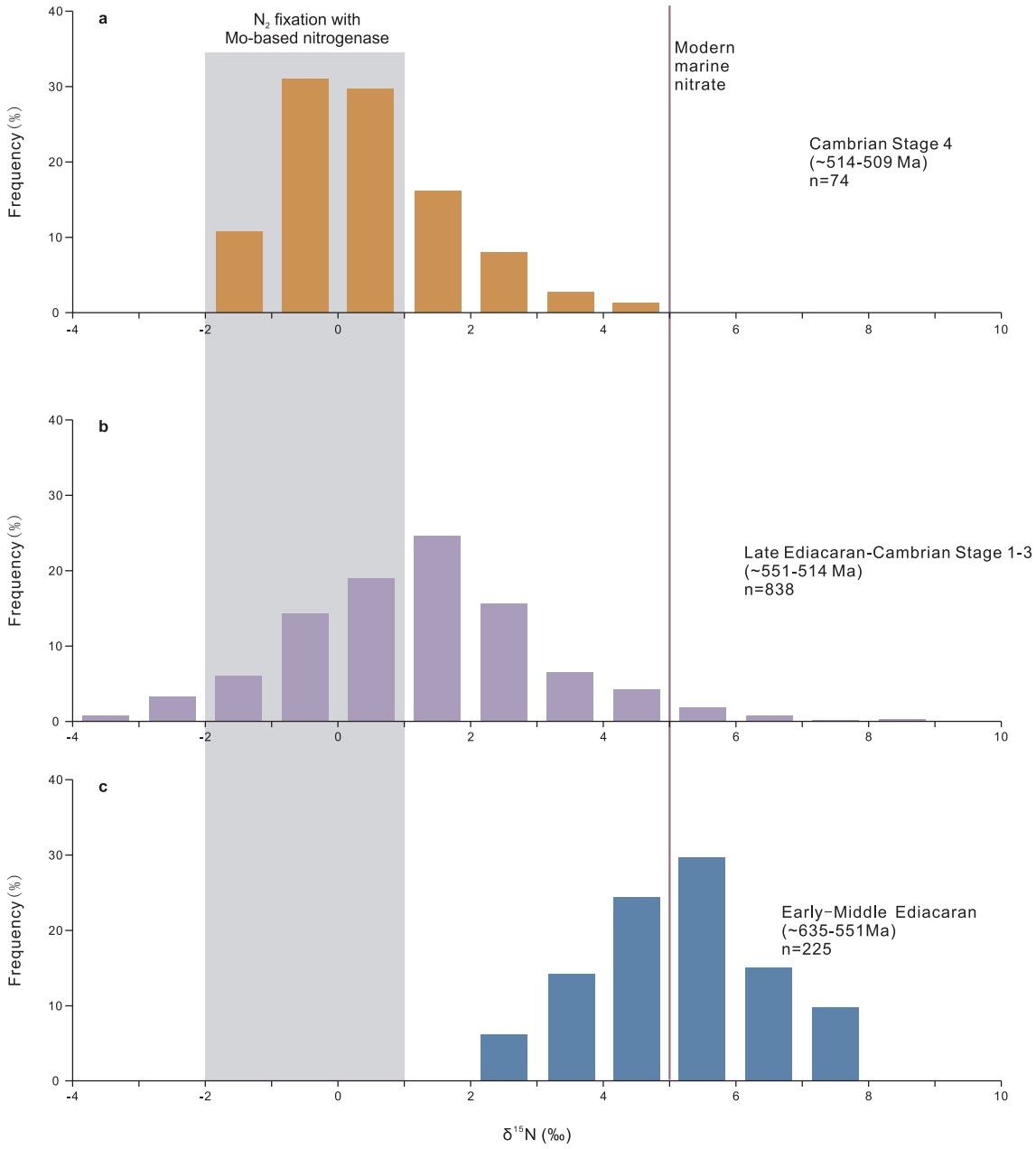

Fig. 5. Distribution of $\delta^{15}N$ values in sedimentary organic matter from the a) Early-Middle Ediacaran, b) Late Ediacaran and Cambrian Stage 1–3, and c) Cambrian Stage 4. Age data and stratigraphic correlation framework follow Steiner et al. (2007), Jiang et al. (2012), and Kouchinsky et al. (2012). Gray highlighted region shows the $\delta^{15}N$ values associated with N fixation using Mo-based nitrogenases; purple vertical line indicates the approximate $\delta^{15}N$ value of modern marine nitrate.

rate (PAR) using Eq. (23) in Schoepfer et al. (2015) are quite low in the Piyuancun Formation ($< 10^4$ mg C cm^{-2} kyr^{-1}; Fig. 4), though they increase substantially in the Hetang Formation, to values comparable to modern marine environments (Fig. 4). While the low values in the Piyuancun Formation might be attributable to low dissolved P concentrations (see below) rather than low productivity *per se*, these estimates are consistent with TOC-based calculations in that they show no notable decrease in productivity associated with the transition toward lower nitrogen isotope values in the middle and upper Hetang Formation.

4.4. Nutrient limitation of primary productivity

As described above (Section 4.2), the predominant nitrogen source fueling phytoplankton productivity during deposition of the Piyuancun Formation and lower Hetang Formation was nitrate. The system transitioned into a mode dominated by N_2 fixation during deposition of the middle and upper Hetang Formation. Notably, this apparent transition in the nitrogen cycle does not correspond with a substantial decrease in calculated productivity, regardless of which method is used, and with some approaches corresponds with a modest increase in calculated productivity. Organic-rich shale and mudstone deposition corresponding with low (< 1‰) $\delta^{15}N$ values was widespread in South China during Cambrian Stages 1–4 (Cremonese et al., 2013, 2014; Kikumoto et al., 2014; Wang et al., 2015; Zhang et al., 2017), suggesting that these low nitrogen isotope values do not reflect an ecological response to increasing nitrogen limitation.

The lack of a relationship between increased nitrogen fixation and calculated productivity indicates that fixed N was likely not the ultimate limiting nutrient during the Ediacaran-Cambrian transition in South China (Falkowski, 1997; Tyrrell, 1999; Michiels et al., 2017). This may be related to the pervasive anoxia that characterized the

waters of the South China Ocean from the Late Ediacaran through Cambrian Stage 3 (Canfield et al., 2008). While anoxic conditions in the modern world are often associated with efficient recycling of sedimentary phosphorus (Van Cappellen and Ingalls, 1994), persistently ferruginous conditions may have promoted effective sequestration of P by adsorption in iron-bearing phases (Reinhard et al., 2017; Laakso and Schrag, 2017), which would diminish P concentrations in the euphotic zone and suppress primary productivity. Phosphorite horizons and nodules have been observed in other areas of the Qiantang Gulf, such as the Jiangshan district, and on the Upper Yangtze platform, at the Xiaotan section (Cremonese et al., 2013), supporting the inference that phosphate was accumulating in authigenic deposits during Cambrian Stages 1–3.

Some paleoproductivity reconstructions show an increase in productivity in the Hetang Formation, or specifically in the upper Hetang Formation. (Fig. 4). Such an increase would likely require an increase in the weathering flux of P. At the same time, the expansion of euxinic water masses in response to increasing biological oxygen demand would promote P regeneration (Brocks et al., 2017), allowing the accumulation of a substantial oceanic dissolved phosphate reservoir. A net increase in the oceanic P reservoir would not only promote the flourishing of the primary producer community, it would also require an expansion of nitrogen fixation in order to maintain Redfieldian nutrient ratios in the photic zone. This may have provided an ecological advantage to cyanobacteria relative to eukaryotic algae, as the former would be able to take advantage of the surplus of available P by fixing atmospheric N_2 (Tyrrell, 1999). While there is no substantial change in the P content of Chunye-1 deposits across this transition (Fig. 2), this may be due to the pervasive anoxia of the depositional environment, which was not favorable to phosphate accumulation regardless of the oceanic phosphate concentration.

4.5. Evolution of primary producers and implications for the Cambrian Explosion

Eukaryotes lack the capacity for biological N_2 fixation, and preferentially assimilate nitrate from the ambient environment; prokaryotes preferentially assimilate ammonium, and some are able to directly fix N_2 in biologically usable species (Anbar and Knoll, 2002; Fawcett et al., 2011; Stüeken et al., 2016; Van Oostende et al., 2017). The apparent dominance of NO_3^- in the euphotic zone from the Late Ediacaran through Cambrian Stages 1–3 would promote the flourishing of a eukaryote dominated phytoplankton community. This is supported by additional lines of evidence, including organic biomarkers (Kunimitsu et al., 2009, Hall et al., 2011), scanning electron microscopy (Guo et al., 2008; Shi et al., 2014; Xu and Li, 2015), and palynological data (Bhattacharya and Dutta, 2015), all of which indicate that eukaryotic algae were the predominant primary producers in this interval.

Biomarker data indicate the emergence of eukaryotic algae prior to the base of the Ediacaran (Brocks et al., 2017). A compilation of published nitrogen isotope measurements from South China, spanning from the Early-Middle Ediacaran to Cambrian Stage 4 (Fig. 5; Table S3; Cremonese et al., 2013, 2014; Ader et al., 2014; Kikumoto et al., 2014; Wang et al., 2013, 2015, 2017; Hammarlund et al., 2017; Zhang et al., 2017), shows a consistent decrease in average $\delta^{15}N$ values from ~5.1‰ in the Early-Middle Ediacaran, through ~1.1‰ during the Late Ediacaran and Cambrian Stages 1–3, and finally to 0.4‰ in Cambrian Stage 4 (Fig. 5, Table S3). This suggests that NO_3^- was the dominant N source fueling phytoplanktonic productivity during the broad Cambrian Explosion interval, from its earliest roots in the Ediacaran (Zhu et al., 2017) through the main episode in Cambrian Stage 3; given their preference for nitrate, eukaryotes may have been the most abundant primary producers in this interval.

Due to the larger cell size and higher proportion of degradation-resistant biomolecules in eukaryotic phytoplankton relative to cyanobacteria (Butterfield, 2009; Lenton et al., 2014; Brocks et al., 2017), a eukaryote-dominated biological pump would promote faster sinking and slower remineralization of organic matter (Lenton et al., 2014). Iron speciation data suggest that pO_2 during the Cambrian Explosion was no higher than 10% of the present-day level (Sperling et al., 2015). An increase in eukaryotic plankton, and thus carbon burial, would have accelerated the accumulation of free oxygen in the ocean, creating new niche space for the evolution of metazoans (Butterfield, 2011; Zhang et al., 2014). Meanwhile, reorganization of nutrient cycles in response to this ecological engineering would promote energy transfer to higher tropic levels (Brocks et al., 2017). Thus, the NO_3^--dominated euphotic zone from the Early-Middle Ediacaran through Cambrian Stage 3 may have facilitated the radiation of relatively large eukaryote phytoplankton, which may have been an important component of early animal diversification.

The observed $\delta^{15}N$ near 0‰ during Cambrian Stage 4 may indicate a decrease in the relative importance of eukaryotes in the primary producer community relative to nitrogen-fixing prokaryotes. The resurgence of a prokaryote-dominated phytoplankton community in the middle to upper Hetang Formation (Cambrian Stage 4) suggests that the replacement of cyanobacteria by eukaryotes was not a unidirectional process during the Neoproterozoic–to-Cambrian transition (Brocks et al., 2017). High primary productivity among picoplankton (0.2–2 μm, Butterfield, 2009) could potentially support large suspension feeders, and the complex pelagic food webs that developed during the Cambrian Explosion (Vinther et al., 2014). Consumption of prokaryotic plankton by suspension feeders would promote the effective burial of organic carbon, and a net increase in atmospheric oxygen, as inferred from Mo- and U-based proxies (Xiang et al., 2017).

5. Conclusions

Striking changes in the sources of nitrogen to the primary producer community occurred between the Late Ediacaran and Cambrian Stage 4, in the Chunye-1 well and across the Yangtze Block. Primary production during deposition of the Piyuancun Formation and lower Hetang Formation was fueled by dissolved NO_3^-, with only a minor contribution from N_2 fixation, whereas the predominant N source for phytoplankton during deposition of the middle and upper Hetang Formation was N_2 fixation. However, primary productivity during Hetang Formation deposition was similar to, or up to an order of magnitude higher than, productivity during deposition of the underlying Piyuancun Formation. Thus, a supply of dissolved nitrate was not in itself a sufficient condition for the flourishing of phytoplankton, and the subsequent transition to a mode dominated by N fixation did not dramatically suppress primary productivity. This suggests that phosphorus or other terrigenous nutrients, rather than nitrogen, may have been the ultimate limiting nutrient during the Ediacaran-Cambrian transition.

Our $\delta^{15}N_{kero}$ results, in combination with published nitrogen isotope data, record a consistent decrease in average $\delta^{15}N$ values, from ~5.1‰ in the Early-Middle Ediacaran, through ~1.1‰ during the Late Ediacaran and Cambrian Stages 1–3, and finally to 0.4‰ in Cambrian Stage 4. Eukaryotes lack the capacity for biological N_2 fixation, and preferentially assimilate nitrate from the ambient environment. Thus, the NO_3^--dominated euphotic zone of the Early-Middle Eadiacaran may have facilitated the development of a eukaryote-dominated phytoplankton community. This community was already established well before the onset of the Cambrian Explosion, and persisted through the peak interval of biological diversification. Thus, while ecological engineering by eukaryotic primary producers was not a proximal cause of the Cambrian Explosion, it may have played an important role in the early diversification of metazoans.

Acknowledgments

We thank Luhua Xie for his assistance with geochemical analyses.

We also thank reviewer Eva Stüeken and editor Randall R. Parrish, for their helpful comments and suggestions to improve the manuscript. This work was supported by the Strategic Priority Research Program (B) of the Chinese Academy of Sciences (XDB18000000), the National Natural Science Foundation of China (Grant nos. 41290260, 41502023, 41273081), and the Key Research Program of Frontier Sciences, Chinese Academy of Sciences.

Appendix A. Supplementary data

Supplementary data associated with this article can be found, in the online version, at http://dx.doi.org/10.1016/j.precamres.2018.05.023.

References

Ader, M., Sansjofre, P., Halverson, G.P., Busigny, V., Trindade, R.I.F., Kunzmann, M., Nogueira, A.C.R., 2014. Ocean redox structure across the late neoproterozoic oxygenation event: a nitrogen isotope perspective. Earth Planet. Sci. Lett. 396, 1–13.

Ader, M., Thomazo, C., Sansjofre, P., Busigny, V., Papineau, D., Laffont, R., Cartigny, P., Halverson, G.P., 2016. Interpretation of the nitrogen isotopic composition of Precambrian sedimentary rocks: assumptions and perspectives. Chem. Geol. 429, 93–110.

Algeo, T.J., Henderson, C.M., Tong, J.N., Feng, Q.L., Yin, H.F., Tyson, R.V., 2013. Plankton and productivity during the Permian-Triassic boundary crisis: an analysis of organic carbon fluxes. Global Planet Change 105, 52–67.

Anbar, A.D., Knoll, A.H., 2002. Proterozoic ocean chemistry and evolution: a bioinorganic bridge? Science 297, 1137–1142.

Beaumont, V., Robert, F., 1999. Nitrogen isotope ratios of kerogens in Precambrian cherts: a record of the evolution of atmosphere chemistry? Precambrian Res. 96, 63–82.

Bhattacharya, S., Dutta, S., 2015. Neoproterozoic-Early Cambrian biota and ancient niche: a synthesis from molecular markers and palynomorphs from Bikaner-Nagaur Basin, Western India. Precambrian Res. 266, 361–374.

Brocks, J.J., Jarrett, A.J.M., Sirantoine, E., Hallmann, C., Hoshin, Y., Liyanage, T., 2017. The rise of algae in Cryogenian oceans and the emergence of animals. Nature 548, 578–581.

Butterfield, N.J., 2009. Oxygen, animals and oceanic ventilation: an alternative view. Geobiology 7, 1–7.

Butterfield, N.J., 2011. Animals and the invention of the Phanerozoic earth system. Trends Ecol. Evol. 26, 81–87.

Cai, C.F., Li, K.K., Ma, A.L., Zhang, C.M., Xu, Z.M., Worden, R.H., Wu, G.H., Zhang, B.S., Chen, L.X., 2009. Distinguishing Cambrian from Upper Ordovician source rocks: evidence from sulfur isotopes and biomarkers in the Tarim Basin. Org. Geochem. 40, 755–768.

Canfield, D.E., Poulton, S.W., Knoll, A.H., Narbonne, G.M., Ross, G., Goldberg, T.S., 2008. Ferruginous conditions dominated later neoproterozoic deep-water chemistry. Science 321, 949–952.

Cremonese, L., Shields-Zhou, G., Struck, U., Ling, H., Och, L., Chen, X., Li, D., 2013. Marine biogeochemical cycling during the early Cambrian constrained by a nitrogen and organic carbon isotope study of the Xiaotan section South China. Precambrian Res. 225, 148–165.

Cremonese, L., Shields-Zhou, G.A., Struck, U., Ling, H., Och, L.M., 2014. Nitrogen and organic carbon isotope stratigraphy of the Yangtze platform during the Ediacaran-Cambrian transition in South China. Paleogeogr. Paleoclimatol. Paleoecol. 398, 165–186.

Erwin, D.H., Laflamme, M., Tweedt, S.M., Sperling, E.A., Pisani, D., Peterson, K.J., 2011. The Cambrian conundrum: early divergence and later ecological success in the early history of animals. Science 334, 1091–1097.

Falkowski, P.G., 1997. Evolution of the nitrogen cycle and its influence on the biological sequestration of CO_2 in the ocean. Nature 387, 272–275.

Fawcett, S.E., Lomas, M., Casey, J.R., Ward, B.B., Sigman, D.M., 2011. Assimilation of upwelled nitrate by small eukaryotes in the Sargasso Sea. Nat. Geosci. 4, 717–722.

Felix, M., 2014. A comparison of equations commonly used to calculate organic carbon content and marine palaeoproductivity from sediment data. Mar. Geol. 347, 1–11.

GBA (Geological Bureau of Anhui), Geological map of Tunxi area Anhui Province. Scale 1 200 1971 000 (in Chinese). 1971.

Glass, J.B., Wolfe-Simon, F., Elser, J.J., Anbar, A.D., 2010. Molybdenum-nitrogen co-limitation in freshwater and coastal heterocystous cyanobacteria. Limnol. Oceanogr. 55, 667–676.

Godfrey, L.V., Falkowski, P.G., 2009. The cycling and redox state of nitrogen in the Archaean ocean. Nat. Geosci. 2, 725–729.

Guo, J.F., Li, Y., Han, J., Zhang, X.L., Zhang, Z.F., Ou, Q., Liu, J.N., Shu, D.G., Maruyama, S., Komiya, T., 2008. Fossil association from the lower Cambrian Yanjiahe formation in the Yangtze Gorges Area, Hubei, South. Acta Geol. Sin. Engl. Ed. 82, 1124–1132.

Hall, P.A., McKirdy, D.M., Halverson, G.P., Jago, J.B., Gehling, J.G., 2011. Biomarker and isotopic signatures of an early Cambrian Lagerstatte in the Stansbury Basin, South Australia. Org. Geochem. 42, 1324–1330.

Hammarlund, E.U., Gaines, R.R., Prokopenko, M.G., Qi, C.X., Hou, X.G., Canfield, D.E., 2017. Early Cambrian oxygen minimum zone-like conditions at Chengjiang. Earth Planet. Sci. Lett. 475, 160–168.

Haq, B.U., Schutter, S.R., 2008. A chronology of Paleozoic sea-level changes. Science 322, 64–68.

Huang, Z.H., Zhang, S.W., 1988. Lithofacies paleogeography of Cambrian Zhejiang Province. Lithofacies Paleogeogr. 33, 13–21 (in Chinese).

Jiang, G.Q., Wang, X.Q., Shi, X.Y., Xiao, S.H., Zhang, S.H., Dong, J., 2012. The origin of decoupled carbonate and organic carbon isotope signatures in the early Cambrian (ca. 542–520 Ma) Yangtze Block. Earth Planet. Sci. Lett. 317–318, 96–110.

Junium, C.K., Arthur, M.A., 2007. Nitrogen cycling during the cretaceous, Cenomanian-Turonian oceanic anoxic event II. Geochem. Geophys. Geosyst. 8, Q03002.

Kikumoto, R., Tahata, M., Nishizawa, M., Sawaki, Y., Maruyama, S., Shu, D.G., Han, J., Komiya, T., Takai, K., Ueno, Y., 2014. Nitrogen isotope chemostratigraphy of the Ediacaran and Early Cambrian platform sequence at Three Gorges South China. Gondwana Res. 25, 1057–1069.

Knoll, A.H., 2017. Food for early animal evolution. Nature 548, 528–530.

Knoll, A.H., Nowak, M.A., 2017. The timetable of evolution. Sci. Adv. 3, e1603076.

Koehler, M.C., Stüeken, E.E., Kipp, M.A., Buick, R., Knoll, A.H., 2017. Spatial and temporal trends in Precambrian nitrogen cycling: a Mesoproterozoic offshore nitrate minimum. Geochim. Cosmochim. Acta 198, 315–337.

Kouchinsky, A., Bengtson, S., Runnegar, B., Skovsted, C., Steiner, M., Vendrasco, M., 2012. Chronology of early Cambrian biomineralization. Geol. Mag. 149, 221–251.

Kump, L.R., Junium, C., Arthur, M.A., Brasier, A., Fallick, A., Melezhik, V., Lepland, A., Crne, A.E., Luo, G.M., 2011. Isotopic evidence for massive oxidation of organic matter following the great oxidation event. Science 334, 1694–1696.

Kunimitsu, Y., Togo, T., Sampei, Y., Kano, A., Yasui, K., 2009. Organic compositions of the embryo-bearing lowermost Cambrian Kuanchuanpu formation on the northern Yangtze platform China. Paleogeogr. Paleoclimatol. Paleoecol. 280, 499–506.

Laakso, T.A., Schrag, D.P., 2017. A theory of atmospheric oxygen. Geobiology 15, 366–384.

Lenton, T.M., Boyle, R.A., Poulton, S.W., Shields-Zhou, G.A., Butterfield, N.J., 2014. Co-evolution of eukaryotes and ocean oxygenation in the Neoproterozoic era. Nat. Geosci. 7, 257–265.

Li, Z.Y., Jia, G.D., 2011. Separation of total nitrogen from sediments into organic and inorganic forms for isotopic analysis. Org. Geochem. 42, 296–299.

Longhurst, A., Sathyendranath, S., Platt, T., Caverhill, C., 1995. An estimate of global primary production in the ocean from satellite radiometer data. J. Plankton Res. 17, 1245–1271.

Maloof, A.C., Porter, S.M., Moore, J.L., Dudas, F.O., Bowring, S.A., Higgins, J.A., Fike, D.A., Eddy, M.P., 2010. The earliest Cambrian record of animals and ocean geochemical change. Geol. Soc. Am. Bull. 122, 1731–1774.

Mángano, M.G., Buatois, L.A., 2014. Decoupling of body-plan diversification and ecological structuring during the Ediacaran-Cambrian transition: evolutionary and geobiological feedbacks. Proc. R. Soc. B Biol. Sci. 281, 20140038.

Michiels, C.C., Darchambeau, F., Roland, F.A.E., Morana, C., Lliros, M., Garcia-Armisen, T., Thamdrup, B., Borges, A.V., Canfield, D.E., Servais, P., Descy, J.P., Crowe, S.A., 2017. Iron-dependent nitrogen cycling in a ferruginous lake and the nutrient status of Proterozoic oceans. Nat. Geosci. 10, 217–221.

Moore, C.M., Mills, M.M., Arrigo, K.R., Berman-Frank, I., Bopp, L., Boyd, P.W., Galbraith, E.D., Geider, R.J., Guieu, C., Jaccard, S.L., Jickells, T.D., La Roche, J., Lenton, T.M., Mahowald, N.M., Maranon, E., Marinov, I., Moore, J.K., Nakatsuka, T., Oschlies, A., Saito, M.A., Thingstad, T.F., Tsuda, A., Ulloa, O., 2013. Processes and patterns of oceanic nutrient limitation. Nat. Geosci. 6, 701–710.

Müller, P.J., Suess, E., 1979. Productivity, sedimentation-rate, and sedimentary organic-matter in the oceans.1 organic-carbon preservation. Deep Sea Res. Part A 26, 1347–1362.

Na, L., Kiessling, W., 2015. Diversity partitioning during the Cambrian radiation. Proc. Natl. Acad. Sci. U.S.A. 112, 4702–4706.

Peters, S.E., Gaines, R.R., 2012. Formation of the 'great unconformity' as a trigger for the Cambrian explosion. Nature 484, 363–366.

Raiswell, R., Canfield, D.E., 2012. The iron biogeochemical cycle past and present. Geochem. Perspect. 1, p22.

Reinhard, C.T., Planavsky, N.J., Gill, B.C., Ozaki, K., Robbins, L.J., Lyons, T.W., Fischer, W.W., Wang, C.J., Cole, D.B., Konhauser, K.O., 2017. Evolution of the global phosphorus cycle. Nature 541, 386–389.

Robinson, R.S., Kienast, M., Albuquerque, A.L., Altabet, M., Contreras, S., Holz, R.D., Dubois, N., Francois, R., Galbraith, E., Hsu, T.C., Ivanochko, T., Jaccard, S., Kao, S.J., Kiefer, T., Kienast, S., Lehmann, M.F., Martinez, P., McCarthy, M., Mobius, J., Pedersen, T., Quan, T.M., Ryabenko, E., Schmittner, A., Schneider, R., Schneider-Mor, A., Shigemitsu, M., Sinclair, D., Somes, C., Studer, A., Thunell, R., Yang, J.Y., 2012. A review of nitrogen isotopic alteration in marine sediments. Paleoceanography 27 Pa4203.

Saltzman, M.R., 2005. Phosphorus, nitrogen, and the redox evolution of the Paleozoic oceans. Geology 33, 573–576.

Schoepfer, S.D., Shen, J., Wei, H.Y., Tyson, R.V., Ingall, E., Algeo, T.J., 2015. Total organic carbon, organic phosphorus, and biogenic barium fluxes as proxies for paleomarine productivity. Earth Sci. Rev. 149, 23–52.

Scott, C., Lyons, T.W., Bekker, A., Shen, Y., Poulton, S.W., Chu, X., Anbar, A.D., 2008. Tracing the stepwise oxygenation of the Proterozoic ocean. Nature 452, 456–459.

Shi, C.H., Cao, J., Hu, K., Bian, L.Z., Yao, S.P., Zhou, J., Han, S.C., 2014. New understandings of Ni-Mo mineralization in early Cambrian black shales of South China: constraints from variations in organic matter in metallic and non-metallic intervals. Ore Geol. Rev. 59, 73–82.

Sigman, D.M., Casciotti, K.L., 2001. Nitrogen isotopes in the ocean. In: Steele, J.H., Turekian, K.K., Thorpe, S.A. (Eds.), Encyclopedia of Ocean Sciences. Academic Press, London, pp. 1884–1894.

Sperling, E.A., Wolock, C.J., Morgan, A.S., Gill, B.C., Kunzmann, M., Halverson, G.P., Macdonald, F.A., Knoll, A.H., Johnston, D.T., 2015. Statistical analysis of iron geochemical data suggests limited late Proterozoic oxygenation. Nature 523, 451–454.

Squire, R.J., Campbell, I.H., Allen, C.M., Wilson, C.J.L., 2006. Did the Transgondwanan Supermountain trigger the explosive radiation of animals on earth? earth planet. Sci. Lett. 250, 116–133.
Stein, R., 1986. Surface-water-paleo-productivity as inferred from sediments deposited in oxic and anoxic deep-water environment of the Mesozoic Atlantic Ocean. In: Degens, E.T. (Ed.), Biogeochemistry of Black Shales. Mitteilungen des Geologisch-Paläontologischen Instituts der Universität, Hamburg, pp. 55–70.
Steiner, M., Li, G.X., Qian, Y., Zhu, M.Y., Erdtmann, B.D., 2007. Neoproterozoic to early Cambrian small shelly fossil assemblages and a revised biostratigraphic correlation of the Yangtze Block (China). Palaeogeogr. Palaeoclimatol. Palaeoecol. 254, 67–99.
Stüeken, E.E., Buick, R., Guy, B.M., Koehler, M.C., 2015. Isotopic evidence for biological nitrogen fixation by molybdenum-nitrogenase from 3.2 Gyr. Nature 520, 666–669.
Stüeken, E.E., Kipp, M.A., Koehler, M.C., Buick, R., 2016. The evolution of earth's biogeochemical nitrogen cycle. Earth Sci. Rev. 160, 220–239.
Stüeken, E.E., Zaloumis, J., Meixnerova, J., Buick, R., 2017. Differential metamorphic effects on nitrogen isotopes in kerogen extracts and bulk rocks. Geochim. Cosmochim. Acta 217, 80–94.
Tyrrell, T., 1999. The relative influences of nitrogen and phosphorus on oceanic primary production. Nature 400, 525–531.
Van Cappellen, P., Ingall, E.D., 1994. Benthic phosphorus regeneration, net primary production, and ocean anoxia – a model of the coupled marine biogeochemical cycles of carbon and phosphorus. Paleoceanography 9, 677–692.
Van Oostende, N., Fawcett, S.E., Marconi, D., Lueders-Dumont, J., Sabadel, A.J.M., Woodward, E.M.S., Jonsson, B.F., Sigman, D.M., Ward, B.B., 2017. Variation of summer phytoplankton community composition and its relationship to nitrate and regenerated nitrogen assimilation across the North Atlantic Ocean. Deep Sea Res. Part I Oceanogr. Res. Pap. 121, 79–94.
Vinther, J., Stein, M., Longrich, N.R., Harper, D.A.T., 2014. A suspension-feeding anomalocarid from the Early Cambrian. Nature 507, 496–499.
Wang, J.G., Chen, D.Z., Yan, D.T., Wei, H.Y., Xiang, L., 2012. Evolution from an anoxic to oxic deep ocean during the Ediacaran-Cambrian transition and implications for bioradiation. Chem. Geol. 306, 129–138.
Wang, W., Guan, C., Zhou, C., Peng, Y., Pratt, L.M., Chen, X., Chen, L., Chen, Z., Yuan, X., Xiao, S., 2017. Integrated carbon, sulfur, and nitrogen isotope chemostratigraphy of the Ediacaran Lantian Formation in South China: Spatial gradient, ocean redox oscillation, and fossil distribution. Geobiology 15, 552–571.
Wang, X.Q., Shi, X.Y., Tang, D.J., Zhang, W.H., 2013. Nitrogen isotope evidence for redox variations at the Ediacaran-Cambrian transition in South China. J. Geol. 121, 489–502.
Wang, D., Struck, U., Ling, H.F., Guo, Q.J., Shields-Zhou, G.A., Zhu, M.Y., Yao, S.P., 2015. Marine redox variations and nitrogen cycle of the early Cambrian southern margin of the Yangtze Platform, South China: evidence from nitrogen and organic carbon isotopes. Precambrian Res. 267, 209–226.
Xiang, L., Schoepfer, S.D., Shen, S.Z., Cao, C.Q., Zhang, H., 2017. Evolution of oceanic molybdenum and uranium reservoir size around the Ediacaran-Cambrian transition: Evidence from western Zhejiang, South China. Earth Planet. Sci. Lett. 464, 84–94.
Xu, J., Li, Y.L., 2015. An SEM study of microfossils in the black shale of the Lower Cambrian Niutitang Formation, Southwest China: implications for the polymetallic sulfide mineralization. Ore Geol. Rev. 65, 811–820.
Xue, Y.S., Yu, C.L., 1979. Petrology and depositional environment analysis of Hetang Formation, Lower Cambrian, western Zhejiang and eastern Jiangxi. Acta Stratigraphica Sin. 3, 283–295 (in Chinese).
Yuan, Y.Y., Cai, C.F., Wang, T.K., Xiang, L., Jia, L.Q., Chen, Y., 2014. Redox condition during Ediacaran-Cambrian transition in the Lower Yangtze deep water basin, South China: constraints from iron speciation and $\delta^{13}C_{org}$ in the Diben section. Chin. Sci. Bull. 59, 3638–3649.
Zerkle, A.L., Poulton, S.W., Newton, R.J., Mettam, C., Claire, M.W., Bekker, A., Junium, C.K., 2017. Onset of the aerobic nitrogen cycle during the great oxidation event. Nature 542, 465–467.
Zhang, J.P., Fan, T.L., Zhang, Y.D., Lash, G.G., Li, Y.F., Wu, Y., 2017. Heterogenous oceanic redox conditions through the Ediacaran-Cambrian boundary limited the metazoan zonation. Sci. Rep. 7, 8550.
Zhang, X.N., Sigman, D.M., Morel, F.M.M., Kraepiel, A.M.L., 2014. Nitrogen isotope fractionation by alternative nitrogenases and past ocean anoxia. Proc. Natl. Acad. Sci. U.S.A. 111, 4782–4787.
Zhu, M.Y., Zhang, J.M., Steiner, M., Yang, A.H., Li, G.X., Erdtmann, B.D., 2003. Sinian-Cambrian stratigraphic framework for shallow- to deep-water environments of the Yangtze Platform: an integrated approach. Prog. Nat. Sci. 13, 951–960.
Zhu, M.Y., Zhuravlev, A.Y., Wood, R.A., Zhao, F.C., Sukhov, S.S., 2017. A deep root for the Cambrian explosion: Implications of new bio-and chemostratigraphy from the Siberian Platform. Geology 45, 459–462.